$CP^1+U(1)$ lattice gauge theory in three dimensions: Phase structure, spins, gauge bosons, and instantons

Shunsuke Takashima and Ikuo Ichinose

Department of Applied Physics, Nagoya Institute of Technology, Nagoya 466-8555, Japan

Tetsuo Matsui

Department of Physics, Kinki University, Higashi-Osaka 577-8502, Japan

In this paper we study a three-dimensional (3D) lattice spin model of CP^1 Schwinger-bosons coupled with dynamical compact $U(1)$ gauge bosons. The model contains two parameters; the gauge coupling and the hopping parameter of CP^1 bosons. At large (weak) gauge couplings, the model reduces to the classical O(3) [O(4)] spin model with long-range and/or multispin interactions. It is also closely related to the recently proposed "Ginzburg-Landau" theory for quantum phase transitions of $s=1/2$ quantum spin systems on a 2D square lattice at zero temperature. We numerically study the phase structure of the model by calculating specific heat, spin correlations, instanton density, and gauge-boson mass. The model has two phases separated by a critical line of second-order phase transition: O(3) spin-ordered phase and spin-disordered phase. The spin-ordered phase is the Higgs phase of $U(1)$ gauge dynamics, whereas the disordered phase is the confinement phase. We find a crossover in the confinement phase which separates dense and dilute regions of instantons. On the critical line, spin excitations are gapless, but the gauge-boson mass is *nonvanishing*. This indicates that a confinement phase is realized on the critical line. To confirm this point, we also study the noncompact version of the model. A possible realization of a deconfinement phase on the criticality is discussed for the $CP^N+U(1)$ model with larger N.

I. INTRODUCTION

The concept of gauge theory plays an important role not only in elementary particle physics but also in condensed-matter physics. In particular, in strongly correlated electron systems and quantum spin systems at quantum phase transitions, unconventional low-energy excitations with "fractional" and/or "exotic" quantum numbers are expected to appear. In order to describe these excitations, gauge-theoretical approaches are sometimes quite useful.

For example, in the fractional quantum Hall effect (FQHE), each electron in a strong magnetic field separates into a so-called composite fermion (CF) and even number of fictitious magnetic flux quanta.[1] Various experiments indicate that the CF's, instead of electrons, behave as quasiparticles. In a gauge-theoretical approach to describing this phenomenon, a gauge field binding each CF and flux quanta is introduced.[2] When the dynamics of this gauge field is realized in a *deconfinement* phase, CF's and flux quanta dissociate each other, and the CF's become quasiparticle moving in an effective magnetic field made of the external magnetic field and the condensation of flux quanta. Then the integer QHE of CF's explains the FQHE. This mechanism of FQHE was called particle-flux separation (PFS), and the critical temperature of confinement-deconfinement transition below which the CF picture holds was estimated.[2]

In the high-T_c superconductivity, a phenomenon called charge-spin separation (CSS) (Ref. 3) was proposed to explain the anomalous behavior of the metallic phase of cuprates. In the CSS scenario, each electron in a cuprate is viewed as a composite of a holon and a spinon. A gauge-

theoretical understanding of the CSS parallels the PFS as a deconfinement phenomenon of the gauge field binding a holon and a spinon.[4,5] Then holons and spinons themselves behave as quasifree particles.

Recently, the importance of quantum phase transitions (QPT's) has been recognized, and several interesting proposals have been made.[6] One of the most tractable systems of QPT's is quantum spin models in low dimensions. By varying some parameters of a quantum spin Hamiltonian, a phase transition from one phase with a certain order (e.g., the Néel order) to another phase with different order (e.g., the dimer) may occur. Then one is interested in what is the low-energy effective theory of the system that corresponds to the Ginzburg-Landau theory (GLT) of a second-order phase transition, and how it describes the phase transition. One may also ask the nature of the low-energy excitations appearing just on the criticality.

For the conventional superconductivity, the GLT is well known and involves a collective scalar field describing Cooper pairs and a gauge field describing electromagnetic (EM) vector potential. The superconducting phase corresponds to the Higgs phase of the EM gauge dynamics, in which gauge bosons (photons) acquire a mass via the Anderson-Higgs mechanism. The normal phase correponds to the Coulomb phase with massless gauge bosons.

For a certain class of quantum $s=1/2$ spin models in two dimensions, it has been proposed that the corresponding "GLT" is a CP^1 model coupled with a dynamical $U(1)$ gauge field.[7] This is quite natural because the path-integral representation involves a set of coherent states of $s=1/2$ quantum spin, which is conveniently labeled by a CP^1 (complex pro-

jective) variable, sometimes called a Schwinger boson. The U(1) gauge field here appears as $s=0$ collective excitations to generate effective interactions between CP^1 spinons.

Then it is an urgent matter to set up a concrete CP^1 model coupled with a U(1) gauge field, and study its phase structure, low-energy excitations, etc. In this paper, we shall consider a three-dimensional (3D) lattice CP^1 model and study its properties by numerical methods very intensively. The model contains two parameters c_1 and c_2; c_1 controls the spin stiffness (the hopping parameter of CP^1 bosons) and c_2 is the inverse gauge coupling constant which controls fluctuations of the U(1) gauge field. This model may be viewed as an effective model of a quantum spin system on a 2D square lattice at zero temperature (T). It is also closely related to the t-J model of the cuprates[4,5] and the gauge-theory approach to heavy fermion systems.[8]

Let us briefly explain the relation between the present model and the t-J model of strongly correlated electrons. In the previous papers,[9] we studied the t-J model in the slave-fermion (SF) representation, in which spinons are described by CP^1 bosons and holons are described by fermions. At the half filling (no holons), the system becomes the 2D $s=1/2$ antiferromagnetic (AF) Heisenberg spin model. At $T=0$ it is described by the 3D CP^1 model with infinite gauge coupling, which is just the present model at $c_2=0$. The model exhibits a phase transition at $c_1=c_{1c}$ between the O(3) spin ordered and disordered phases[4] (see Secs. II B and IV for more details). In lightly doped cases, holons can be integrated to "renormalize" the spin-stiffness constant c_1 and destroy the long-range Néel order as the holon density increases.[9] For larger dopings, holons generate nontrivial interactions between the gauge bosons. Such a system may be mimicked to a certain extent by the present model with a suitable amount of the c_2 term (see Sec. II B ii), although one needs certainly more quantitative study on this point.

The rest of the paper is organized as follows. In Sec. II, we shall introduce the model and explain its relations to the classical O(3) and O(4) nonlinear sigma models, the GLT for quantum spin models, etc. In Sec. III, we study the phase diagram by mean-field theory (MFT). In Sec. IV, we calculate the specific heat and present the global phase diagram of the model in the c_2-c_1 plane. The model exhibits a second-order phase transition along the critical line $c_1=c_{1c}(c_2)$, which separates the confinement phase and the Higgs phase. In Sec. V, we study spin-spin correlation functions. The results show that the observed phase transition accompanies a spontaneous magnetization and the spin excitations are gapless on the critical line as well as in the spin-ordered phase. In Sec. VI, we calculate instanton (monopole) density in various places in the phase diagram. This supplies us with useful information to understand the gauge dynamics. In Sec. VII, we measure the gauge-boson mass by calculating gauge-invariant correlation functions of field strength. Two mechanisms of generating a gauge-boson mass are explained: (i) condensation of instantons, and (ii) Anderson-Higgs mechanism by condensation of the CP^1 variables. We also obtain the gauge-boson mass in $\lambda\phi^4$ Higgs models and compare the results with the previous calculations in order to check the present calculations. Section VIII is devoted to discussion.

II. 3D CP^1+U(1) LATTICE GAUGE MODEL

A. Model

Let us define the CP^1+U(1) gauge model on the cubic lattice. We use x as the site index, and $\mu=0,1,2$ as the direction index. We use μ also as the unit vector in the μth direction. On each site x we have a CP^1 variable z_x, which is a two-component complex number,

$$z_x \equiv \begin{pmatrix} z_{x1} \\ z_{x2} \end{pmatrix}, \quad z_{x1}, z_{x2} \in C, \tag{2.1}$$

satisfying the CP^1 constraint,

$$\sum_{a=1}^{2} |z_{xa}|^2 = 1. \tag{2.2}$$

On each link $(x, x+\mu)$ we have a U(1) gauge variable, $U_{x\mu} = \exp(i\theta_{x\mu})[\theta_{x\mu} \in (-\pi, +\pi)]$.

The partition function Z of the model is written as

$$Z = \int [dU] \int [dz] \exp(-S),$$

$$[dU] \equiv \prod_{x,\mu} dU_{x\mu} = \prod_{x,\mu} \frac{d\theta_{x\mu}}{2\pi},$$

$$[dz] \equiv \prod_x dz_{x1} dz_{x2} \delta(|z_{x1}|^2 + |z_{x2}|^2 - 1). \tag{2.3}$$

The action S of the model is given by

$$S = -\frac{c_1}{2} \sum_{x,\mu,a} (\bar{z}_{x+\mu,a} U_{x\mu} z_{xa} + \text{H.c.})$$

$$-\frac{c_2}{2} \sum_{x,\mu<\nu} (\bar{U}_{x\nu} \bar{U}_{x+\nu,\mu} U_{x+\mu,\nu} U_{x\mu} + \text{H.c.}), \tag{2.4}$$

where c_1 and c_2 are real parameters of the model.

The action S is invariant under the following U(1) local (x-dependent) gauge transformation:

$$z_{xa} \rightarrow z'_{xa} = \exp(i\Lambda_x) z_{xa},$$

$$U_{x\mu} \rightarrow U'_{x\mu} = \exp(i\Lambda_{x+\mu}) U_{x\mu} \exp(-i\Lambda_x). \tag{2.5}$$

A genuine CP^1 variable is characterized by (i) the constraint (2.2) and (ii) the redundancy under the phase transformation $z_{xa} \rightarrow \exp(i\Lambda_x) z_{xa}$. The gauge symmetry (2.5) assures us of this redundancy.

Besides the above local gauge symmetry, S has a symmetry under the following global SU(2) transformation:

$$z_x \rightarrow V z_x, V \in \text{SU}(2). \tag{2.6}$$

This induces the global O(3) spin rotation, which shall be explained in the following subsection, part (ii).

B. Special cases

The present model reduces to some known models in certain limits of the parameters.

(i) Pure gauge model ($c_1=0$). For $c_1=0$ the model reduces to the 3D compact U(1) gauge model without matter couplings, where c_2 is the inverse of the gauge coupling constant g, i.e., $c_2 \propto g^{-2}$. Polyakov[10] showed that this model stays always in the confinement phase regardless of the value of c_2 due to the condensation of instantons (monopoles). We shall study the instanton effect and verify his result by numerical calculation in Sec. VI.

(ii) O(3) spin model ($c_2=0$). For $c_2=0$ the model reduces to a O(3) nonlinear sigma model (classical Heisenberg spin model) with a modified action. Here one can perform the integration over $U_{x\mu}$ exactly because the plaquette coupling between $U_{x\mu}$'s disappears. One obtains

$$Z = \int [d\vec{S}] \exp\left[\sum_{x,\mu} \ln I_0\left(c_1 \sqrt{\frac{1+\vec{S}_{x+\mu}\cdot\vec{S}_x}{2}} \right) \right], \quad (2.7)$$

with the following measure:

$$[d\vec{S}] = \prod_x \prod_{i=1}^3 \delta\left(\sum_{i=1}^3 S_{xi}^2 - 1 \right), \quad (2.8)$$

where $I_0(\gamma)$ is the modified Bessel function. $\vec{S}_x$ is a three-component O(3) classical spin vector, made of the CP^1 variable

$$\vec{S}_x = \bar{z}_x \vec{\sigma} z_x, \quad \vec{S}_x \cdot \vec{S}_x = 1, \quad (2.9)$$

where $\vec{\sigma}$ is the 2×2 Pauli spin matrices. We note that $\vec{S}_x$ is a gauge-invariant object. A global O(3) rotation of $\vec{S}_x$, which is a symmetry of the model, is induced by a global SU(2) transformation of z_x,

$$\vec{S}_x \rightarrow \Omega \vec{S}_x, \Omega \in O(3),$$

$$z_x \rightarrow V z_x, V \in SU(2). \quad (2.10)$$

In Eq. (2.9) we have used the relation $[dz]f(\{\bar{z}_x\vec{\sigma}z_x\}) = [d\vec{S}]f(\{\vec{S}_x\})$. Since $\ln I_0(\gamma)$ is a monotonically increasing function of γ, it is almost obvious that the model (2.7) belongs to the same universality class as the standard O(3) model with the action $-J\sum \vec{S}_{x+\mu}\cdot\vec{S}_x$. Then the model (2.7) should exhibit a second-order phase transition at a certain critical value $c_1=c_{1c}[O(3)]$, which separates the O(3) spin-ordered phase and the disordered phase. It is obvious from Eq. (2.7) that the parameter c_1 controls the spin stiffness.

For small c_2, integration over the gauge field $U_{x\mu}$ can be done perturbatively in powers of c_2. The plaquette term in Eq. (2.4) generates four-spin couplings like $(\vec{S}_{x+\mu}\cdot\vec{S}_x) \times (\vec{S}_{x+\mu+\nu}\cdot\vec{S}_{x+\nu})$ in the leading order of c_2, which prefer a ferromagnetic order for $c_2 > 0$. The higher-order terms of c_2 become nonlocal and contain many spin variables.

For any finite value of c_2, integration over the gauge field $U_{x\mu}$ in the partition function Z in Eq. (2.3) results in an effective spin model $S_{SM}(\vec{S}_x)$,

$$\int [d\vec{S}]\exp(-S_{SM}) = \int [dU] \int [dz]\exp(-S), \quad (2.11)$$

because the "spin variable" $\vec{S}_x$ is the only gauge-invariant object made of $z_{x\alpha}$. In later discussions, we call the off-diagonal long-range order of $\vec{S}_x$ magnetization since it measures a spontaneous breakdown of the SU(2) or O(3) global symmetry (2.10). Later numerical calculation shows that there exists a second-order phase transition in the present model for which $\vec{S}_x$ works as an order parameter.

(iii) O(4) spin model ($c_2=\infty$). In the limit $c_2 \rightarrow \infty$, fluctuations of $U_{x\mu}$ are totally suppressed and $U_{x,\mu}$ is restricted to pure gauge configurations, i.e., $U_{x\mu}=\exp(-i\Lambda_{x+\mu})\exp(i\Lambda_x)$. Then Z is reexpressed in terms of four-component O(4) classical spin variables $R_{x\alpha}(\alpha=1,2,3,4) \in R$,

$$z_{x1} = R_{x1} + iR_{x2}, \quad z_{x2} = R_{x3} + iR_{x4},$$

$$\bar{z}_x z_x = \sum_{\alpha=1}^4 R_{x\alpha}^2 = 1,$$

$$[dz] = [d\vec{R}] = \prod_x \prod_{\alpha=1}^4 dR_{x\alpha} \cdot \delta\left(\sum_\alpha R_{x\alpha}^2 - 1 \right) \quad (2.12)$$

as

$$Z = \int [dR]\exp\left(c_1 \sum_{x,\mu} \vec{R}_{x+\mu}\vec{R}_x \right). \quad (2.13)$$

This model is just the 3D nonlinear O(4) sigma model which exibits also a second-order phase transition at $c_1=c_{1c}[O(4)]$, which separates the O(4) spin-ordered phase and the disordered phase.

C. Nonuniform AF Heisenberg model

Let us explain how the model Eq. (2.4) is related to the recently proposed effective-field theories (GLT's) for the *quantum magnets*. In Ref. 11, we studied a phase transition from the Néel state to the dimer state in the nonuniform $s = \frac{1}{2}$ AF Heisenberg model on a square lattice,

$$H_{AF} = \sum_{x,j} J_{xj}\hat{\vec{S}}_x \cdot \hat{\vec{S}}_{x+j}, \quad (2.14)$$

where j is the spatial direction index ($j=1,2$), $\hat{\vec{S}}_x$ is the quantum spin operator at site x, and J_{xj} is the nonuniform exchange coupling. We rename the even lattice sites $x=(o,i)$ where o denotes each odd site, and the index $i=1,2,3$, and 4 specifies its four nearest-neighbor (NN) even sites (see Fig. 1).

The exchange couplings $J_{xj}=J_{oi}$ may be position dependent, and in Ref. 11 we explicitly considered the following dimer configuration:
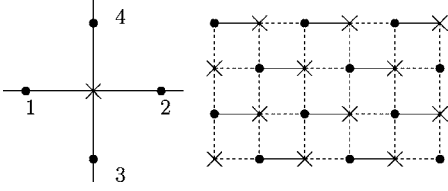
$$J_{oi} = J + \Delta J_{oi},$$

FIG. 1. 2D square lattice; crosses are odd sites and filled circles are even sites. Solid bonds indicate that their exchange couplings are stronger than those on dotted bonds.

$$\Delta J_{oi} = \begin{cases} \Delta J_{oi} = \alpha J, & i = 1 \\ \Delta J_{oi} = -\alpha J, & i = 2,3,4, \end{cases} \quad (2.15)$$

where $0 \le \alpha \le 1$ is a parameter which interpolates between the uniform Heisenberg model ($\alpha=0$) and the dimer model ($\alpha=1$). Its effective-field theory is derived by the standard method[9,12] in path-integral formalism by integrating over the odd-site spins. It takes a form of a CP^1 model in $(2+1)$ dimensions (the extra one dimension is the direction along the imaginary time). Namely, the effective theory has the form of Eq. (2.4), where the effective parameter c_1 is expressed in terms of α and the lattice spacing a as

$$c_1 = \frac{1}{2\sqrt{2}a} \frac{1-\alpha}{2-\alpha} \sqrt{\frac{2(2+\alpha)}{1-\alpha}}. \quad (2.16)$$

The bare effective parameter c_2 is vanishing in this effective-field theory.

As explained in case (ii) above, the model with $c_2=0$ exhibits a second-order phase transition at $c_1=c_{1c}[O(3)]$. Through the correspondence (2.16), this transition from the ordered state to the disordered state of the CP^1 model describes the transition of the nonuniform AF magnet from the Néel state to the dimer state.[13] In Ref. 11 we pointed out the possibility that the *spinons* z_{xa} ($a=1,2$) appear as gapless excitations *at the critical point*. That is, a deconfinement phase like the Coulomb phase in $(3+1)$ dimensions is realized there because of the appearance of long-range correlations among the gauge field. In this paper, among others, we shall reexamine this point, i.e., investigate the possibility whether the Coulomb phase is realized on the critical line of the model (2.4).

D. Uniform AF Heisenberg model with ring exchange

In the framework of the uniform AF Heisenberg model with multiple spin ring exchange, Senthil *et al.*[7] argued that a phase transition from the Néel state to valence bond solid (VBS) takes place. They suppose that the system in the Néel state but near the *critical point* is described by a CP^1 field coupled to a *noncompact* U(1) gauge field, where nonperturbative contributions from instantons are totally suppressed. An effective-field theory in the continuum space-time in this region was given by[7]

$$\mathcal{L}_{\text{deconfine}} = |(\partial_\mu - iA_\mu)\tilde{z}_a|^2 + s|\tilde{z}_a|^2 + u(|\tilde{z}_a|^2)^2 + \frac{1}{g^2}(\epsilon_{\mu\nu\lambda}\partial_\nu A_\lambda)^2,$$
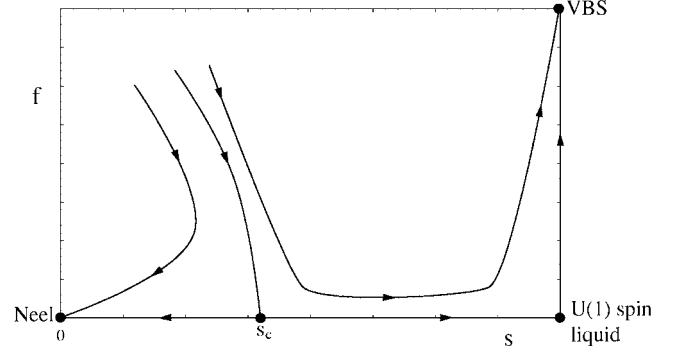
$$(2.17)$$

FIG. 2. Renormalization-group flows of the effective gauge theory of the AF Heisenberg model with the ring exchange (Ref. 7). The horizontal axis refers to the parameter s, and the vertical line to the instanton fugacity f.

where $\tilde{z}_a$ ($a=1,2$) are *unconstrained* complex scalar fields coming from the CP^1 spin variables, A_μ is the gauge potential, and s and u are parameters. For $s < s_c$, $\tilde{z}_a$ are condensed $\langle\tilde{z}_a\rangle \neq 0$ which corresponds to the long-range Néel order. The gauge dynamics is in the Higgs phase and the gauge bosons acquire a mass gap $|\langle\tilde{z}\rangle|$. At the criticality $s=s_c$, $\langle\tilde{z}_a\rangle=0$, whereas the effect of instantons is negligible because of the cancellation mechanism via the Berry phase term.[14] On the other hand, in the VBS state, the instantons are relevant and proliferate to generate the confinement phase. The proposed phase diagram[7] of the AF Heisenberg model is shown in Fig. 2. We shall compare it with that of the present model in Sec. VII C.

III. MEAN-FIELD THEORY

Before going into detailed numerical studies of the model, let us apply a MFT to the model to obtain a rough phase diagram.

The MFT below is based upon the variational principle.[15] We start with the variational action S_0 and use the following relations:

$$Z_0 \equiv \int [dz][dU]\exp(-S_0) \equiv \exp(-F_0),$$

$$F \equiv -\ln Z \le F_v \equiv F_0 + \langle S - S_0 \rangle_0,$$

$$\langle O \rangle_0 \equiv Z_0^{-1} \int [dz][dU] O \exp(-S_0). \quad (3.1)$$

From this Jensen-Peierls inequality, we adjust the variational parameters contained in S_0 optimally so that F_v is minimized.

For the trial action S_0, we assume the translational invariance and consider the following sum of single-site and single-link energies:

$$S_0 = -\frac{1}{2}\sum_x \left(\sum_\mu \bar{W}U_{x\mu} + \sum_a \bar{H}_a z_{xa} + \text{c.c.} \right), \quad (3.2)$$

where W and H are complex variational parameters. Then we obtain the following free energy per site, $f_v \equiv F_v/N$, where N
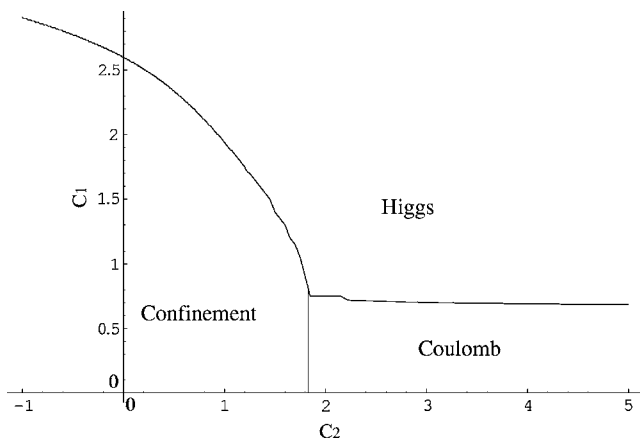
FIG. 3. Phase diagram of the 3D CP^1+U(1) model in MFT. There are three (Higgs, confinement, Coulomb) phases.

is the total number of the 3D lattice sites (we present the formulas for the d-dimensional lattice):

$$h \equiv |H|, \quad \omega \equiv |W|,$$

$$f_v = -d \ln(I_0(\omega)) - \ln[I_0(h) - I_2(h)] - c_1 dm^2 p - c_2 \frac{d(d-1)}{2} p^4$$

$$+ d\omega p + hm,$$

$$m \equiv \left(\sum_a |\langle z_{xa} \rangle_0|^2 \right)^{1/2} = \frac{1}{2} \frac{I_1(h) - I_3(h)}{I_0(h) - I_2(h)},$$

$$p \equiv |\langle U_{x\mu} \rangle_0| = \frac{I_1(\omega)}{I_0(\omega)}, \tag{3.3}$$

where $I_n(\gamma)$ (n is an integer) is the modified Bessel function,

$$I_n(\gamma) = \int_0^{2\pi} \frac{d\theta}{2\pi} \exp(\gamma \cos\theta + in\theta). \tag{3.4}$$

The stationary conditions for f_v with respect to ω, h read

$$\omega = c_1 m^2 + 2c_2(d-1)p^3 + 6c_3(d-1)m^2 p^2,$$

$$h = 2dc_1 mp + 4c_3 d(d-1)mp^3. \tag{3.5}$$

The MFT equations (3.3)–(3.5) for $d=3$ predict the existence of the three phases characterized as follows:

$$\text{phase:} p = \langle U_{x\mu} \rangle, m = \langle z_x \rangle;$$

$$\text{Higgs:} \neq 0, \neq 0;$$

$$\text{Coulomb:} \neq 0, 0;$$

$$\text{confinement:} \quad 0, 0. \tag{3.6}$$

The naming of each phase should be clear. We note that the fourth combination $p=0$ and $m \neq 0$ is missing.

In Fig. 3, we plot the phase boundaries obtained from Eqs. (3.3)–(3.5). The phase boundary of the MFT between
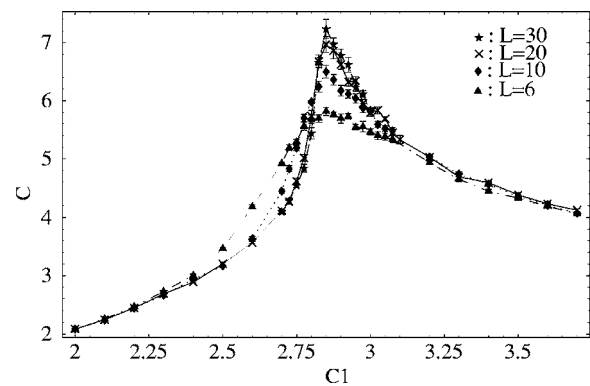

FIG. 4. System-size dependence of the specific heat for $c_2=0$.

the Higgs and Coulomb phases is of second order, whereas the other two boundaries, the Higgs-confinement and confinement-Coulomb, are of first order. Across the second-order transition, p and m vary continuously, while across the first-order transitions, p and/or m change discontinuously with finite jumps of Δp and/or Δm. For the Higgs-confinement transition, $\Delta p \neq 0$ and $\Delta m \neq 0$, and for the confinement-Coulomb transition, $\Delta p \neq 0$ and $\Delta m = 0$, since $m=0$ in both phases.

The present MFT for the CP^1+U(1) model may have some inappropriate points:

(i) As explained above, for the pure gauge case $c_1=0$, the confinement phase should survive up to $c_2 \to \infty$ and the Coulomb phase in the MFT should disappear. In fact, we verify the nonexistence of the Coulomb phase in the following section. However, we shall see some crossover phenomena close to this fictitious transition line (see later discussion).

(ii) At $c_2=0$, the system reduces to the O(3) spin model (2.7) having a second-order transition at $c_1=c_{1c}[\text{O}(3)]$. Thus the first-order transition of the MFT at $c_2=0$ is incorrect. This MFT result should be modified by Monte Carlo simulations in the following section.

On the other hand, in the limit $c_2 \to \infty$, the MFT correctly predicts the order of transition, i.e., the second-order one of the O(4) spin model.

IV. PHASE STRUCTURE

To study the phase structure of the model numerically, we performed Monte Carlo simulations with the Metropolis algorithm for the 3D cubic lattice of the size up to $N=L^3 = 30^3$ with the periodic boundary condition (PBC).

We first calculated thermodynamic quantities per site like the internal energy U and the specific heat C,

$$U = \langle S \rangle / N,$$

$$C = \langle (S - \langle S \rangle)^2 \rangle / N, \tag{4.1}$$

as functions of the parameters c_1 and c_2. The specific heat C has a peak as a function of c_1 for each fixed c_2; see Fig. 4 for $c_2=0$ and Fig. 5 for $c_2=2.0$. These peaks develop as the lattice size increases as $N=6^3, 10^3, 20^3$, and 30^3 for the c_2

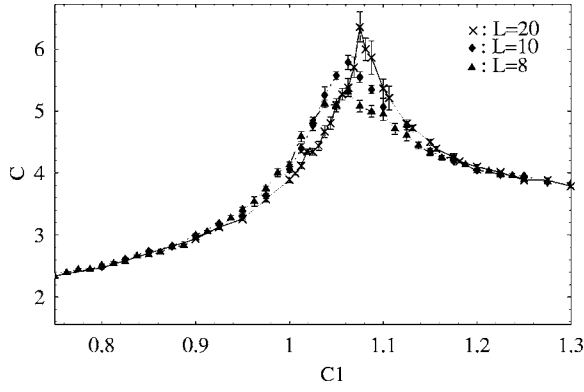FIG. 5. System-size dependence of the specific heat for c_2 $=2.0$.

$=0$ case and $N=8^3, 10^3$, and 20^3 for the $c_2=2.0$, respectively. This behavior indicates second-order phase transitions. Figure 4 shows that the O(3) spin model of Eq. (2.7) has a phase transition at $c_{1c}[\text{O}(3)]=2.85\ldots$.

It is interesting to see if the data of the specific heat exhibit the finite-size scaling (FSS) behavior. Let us introduce a parameter ϵ as

$$\epsilon \equiv \frac{c_1 - c_{1\infty}}{c_{1\infty}}, \qquad (4.2)$$

where $c_{1\infty}$ is the critical coupling at the infinite volume limit. The correlation function ξ behaves as $\xi \propto \epsilon^{-\nu}$ with a critical exponent ν. It is also expected that the peak of C diverges as $C_\infty \propto \epsilon^{-\sigma}$ as $N \to \infty$ with another exponent σ. Then for sufficiently large systems, we expect

$$C_N(\epsilon) = N^{\sigma/\nu} \phi(N^{1/\nu}\epsilon), \qquad (4.3)$$

where $C_N(\epsilon)$ is the specific heat in the system of size N and $\phi(x)$ is a scaling function. We show the scaling functions ϕ in Fig. 6 which are determined from the data in Figs. 4 and 5. The parameters of the FSS are $c_{1\infty}=2.87$, $\nu=1.50$, $\sigma=0.20$ for $c_2=0$ and $c_{1\infty}=1.09$, $\nu=1.17$, $\sigma=0.17$ for $c_2=2.0$, respectively. We think that the finite-size scaling hypothesis (FSSH) holds quite well for the $c_2=0$ case. For the $c_2=2.0$ case, data exhibit the FSS in a smaller parameter region close to the peaks of C than that of the $c_2=0$ case. We think that it
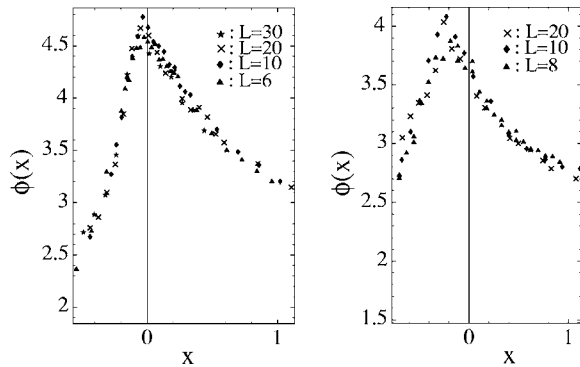
is due to the existence of another length scale besides the spin correlation length ξ, i.e., the correlation length of the gauge boson. See the discussion in Sec. VII.

Next, in Fig. 7, we plot C at $c_1=0$ as a function of c_2. It certainly has a peak at $c_2=1.4\ldots$, which, however, does not develop as the lattice size increases. Thus this peak does not indicate any phase transition along $c_1=0$. This nondeveloping peak at $(c_1=0, c_2=1.4\ldots)$ continues to the region $c_1>0$. This line of the peaks may exhibit some crossover. The physical meaning of this line will be discussed after calculating the instanton density in Sec. VI.

In Fig. 8 we present the phase diagram in the c_2-c_1 plane obtained via these specific-heat measurements. We also show the locations of the nondeveloping peaks as crossovers.

V. SPIN EXCITATIONS

In this section we study the spin-spin correlation functions and the energy gap of spin excitations. The correlator of O(3) spins, $\vec{S}_x$ of Eq. (2.9), is defined as

$$C_S(t) = \langle \vec{S}_x \cdot \vec{S}_{x+t\mu} \rangle. \qquad (5.1)$$

$C_S(t)$ is a function of the distance t but does not depend on the reference point x nor on the direction μ due to the PBC on the cubic lattice.

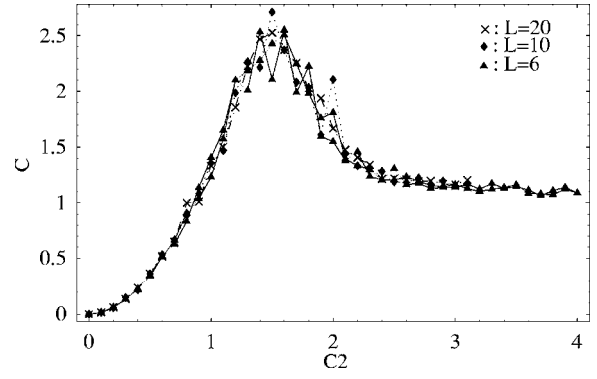Let us first consider the case $c_2=0$. As explained before, this case corresponds to the nearest-neighbor spin model
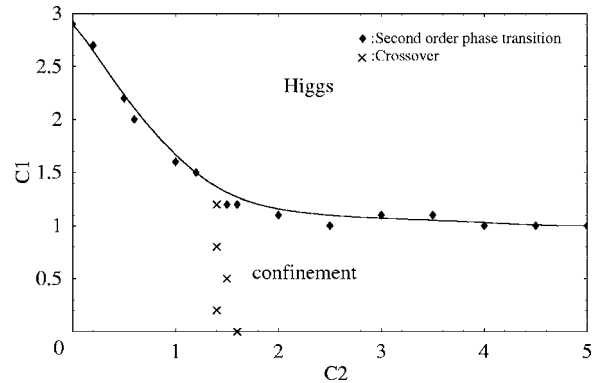

FIG. 7. System-size dependence of the specific heat peak for $c_1=0$. No developments of peaks are observed.

FIG. 6. Scaling function $\phi(x)$ obtained from the data of the c_2 $=0$ (left) and $c_2=2.0$ (right) cases.

FIG. 8. The phase structure of the $CP^1+U(1)$ model in the c_1-c_2 plane obtained by the measurement of the specific heat.
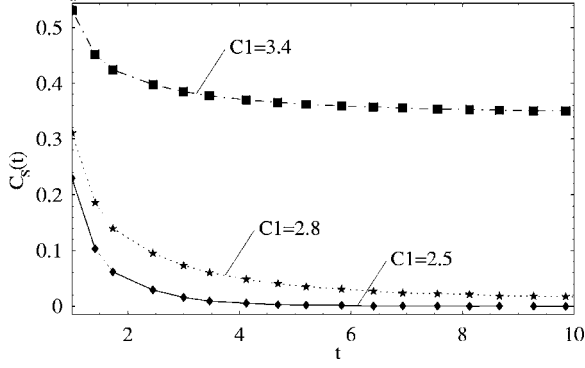
FIG. 9. Spin-spin correlations for $c_2=0$. For $c_1=2.5$, an exponential decay $A' \exp^{-\gamma' t}$ fits it better. For $c_1=2.8$ and 3.4, an algebraic decay $M^2 + At^{-\alpha'}$ fits it better.

(2.7). In Fig. 9 we plot $C_S(t)$ for the lattice size 20^3. $C_S(t)$ changes its behavior around $c_1 = c_{1c}[O(3)] = 2.8\ldots$, the critical point determined by the location of specific heat of Fig. 4. At a higher $c_1 = 3.4 (> c_{1c}[O(3)])$, $C_S(t)$ exhibits a nonvanishing off-diagonal long-range order (magnetization) M, $M^2 \equiv \lim_{t\to\infty} C_S(t)$, where $t \to \infty$ implies $t = L/2$ for a finite lattice of size $N = L^3$. $C_S(t)$ approaches to M^2 algebraically,

$$C_S(t) = M^2 + At^{-(1+\eta')},$$

$$\eta' = 0.0 \sim 0.1 \text{ for } L = 20. \qquad (5.2)$$

In contrast, at a lower $c_1 = 2.5 (< c_{1c}[O(3)])$, $M = 0$ and $C_S(t)$ decays exponentially,

$$C_S(t) = A' \exp(-\gamma' t). \qquad (5.3)$$

Thus the phase transition observed in the previous section corresponds to a spontaneous symmetry breaking of the SU(2) spin symmetry (2.10) of z_x, say $\langle z_x \rangle = (M^{1/2}, 0)^t$. To confirm this observation, we plot the magnetization M for $c_2 = 0$ in Fig. 10. It exhibits a typical behavior of second-order phase transition.

In Fig. 11 we also show the magnetization M at various values of c_2. M starts to develop at the critical points observed by the specific-heat measurement. This means that M
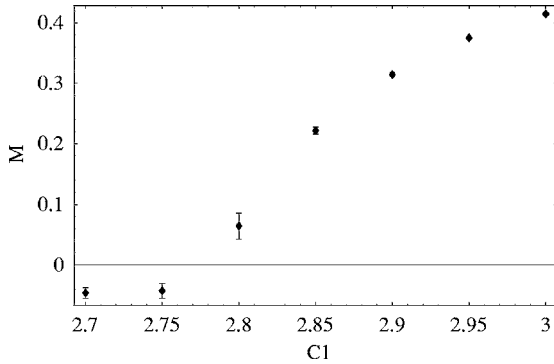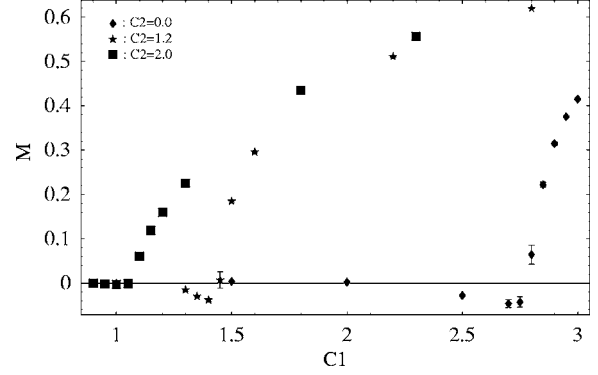

FIG. 11. Spontaneous magnetization for various c_2. The result shows a typical behavior of second-order phase transition.

is an order parameter for the phase transition in the present model.

As we mentioned in Sec. II, the model reduces to the O(4) spin model in the limit $c_2 \to \infty$. We studied the phase structure of this O(4) model, and found that there exists a second-order order-disorder phase transition as in the pure CP^1 model. The critical coupling is estimated as $c_{1c}[O(4)] = 1.0\ldots$ which is fairly close to the critical value of c_1 for sufficiently large c_2. We also investigate the spin-correlation function in the ordered phase. The data can be fitted well in the form (see Fig. 12)

$$C_S(t) = M^2 + bt^{-(1+\eta'')},$$

$$\eta'' = 0.1 \sim 0.3 \text{ for } L = 20. \qquad (5.4)$$

This result indicates that smooth transfer in the behavior of $C_S(t)$ occurs from the O(3) spin model at $c_2 \simeq 0$ to the O(4) spin model at $c_2 \simeq \infty$.

Next let us study the mass (energy gap) M_S of spin excitations. To measure M_S with good precision, we introduce a Fourier transform of the spin variables $\vec{S}_x$ in the 2D plane (x_1, x_2),
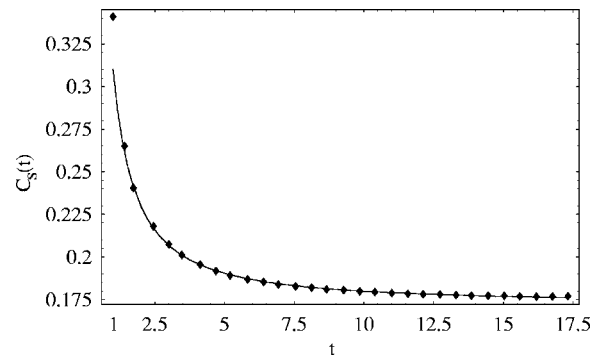

FIG. 10. Spontaneous magnetization for $c_2=0$. The result shows a typical behavior of second-order phase transition.

FIG. 12. Spin-correlation function in the O(4) model at $c_1 = 1.60$ and $c_2 = \infty$. The system size $L = 20$, and the exponent is estimated as $\eta'' = 0.26$.
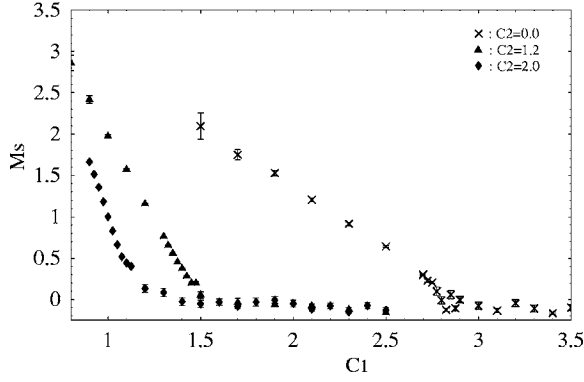
FIG. 13. Energy gap M_S of O(3) spin excitations for $c_2=0.0$, 1.2, and 2.0. The errors become larger for smaller c_1 because of more rapid falloff of $D_S(t)$.

FIG. 14. Instanton distribution is measured at various places [(a)–(l)] in the phase diagram in the c_2-c_1 plane.

$$\widetilde{\vec{S}}(x_3;p_1,p_2) = \sum_{x_1,x_2} e^{ip_1x_1+ip_2x_2}\vec{S}_x. \quad (5.5)$$

In the continuum limit, one can readily find that the correlator of $\widetilde{\vec{S}}(x_3;p_1,p_2)$ behaves as

$$\langle \widetilde{\vec{S}}(x_3;p_1,p_2) \cdot \widetilde{\vec{S}}(0;-p_1,-p_2)\rangle = \int dp_3 \frac{e^{ip_3x_3}}{\vec{p}^2+M_S^2}$$

$$\propto e^{-\sqrt{p_1^2+p_2^2+M_S^2}x_3}, \quad (5.6)$$

where $\vec{p}^2=\Sigma_{i=1,2,3}p_i^2$ and M_S is the energy gap of the lowest spin excitations. Below we fit the measured correlation function on the lattice by using this form to calculate M_S. Let us define

$$D_S(t) = \frac{1}{L^3}\sum_{x_3} \langle \widetilde{\vec{S}}(x_3+t;p_1,p_2) \cdot \widetilde{\vec{S}}(x_3;-p_1,-p_2)\rangle. \quad (5.7)$$

The PBC restricts the momentum as $p_i=2\pi n_i/L$, $n_i=0,1,2,\ldots,L-1$. In the simulation we choose nonvanishing smallest values, $p_1=p_2=2\pi/L$, in order to fit the result in an exponentially decaying form even for $M_S=0$. We note that, from the above definition of M_S, it is possible that M_S^2 takes a negative value as long as the exponent $p_1^2+p_2^2+M_S^2 < 2(2\pi/L)^2$. We shall comment on this point later on.

In Fig. 13, we plot M_S for $N=20^3$. For a fixed c_2, M_S is a smooth function of c_1 and vanishes in the spin ordered phase $c_1>c_{1c}$ as predicted by the Nambu-Goldstone theorem. We checked the result of Fig. 13 by repeating the calculation with the choice $(p_1,p_2)=(2\pi/L,0)$. We shall use the same techniques for calculating the gauge-boson mass in the following section.

VI. INSTANTONS

A. Definition of instanton density

In this section, we calculate the instanton density Q_x at x in various sets of (c_2,c_1). Measurement of Q_x provides us with important information about fluctuations of the gauge field, though it is rather difficult to determine a location of phase transition by itself.
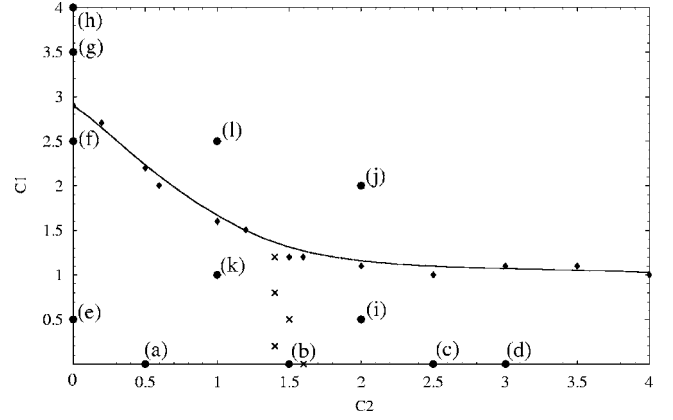
We follow the definition of integer instanton charge by DeGrand and Toussaint.[16] First, let us consider the magnetic flux $\Theta_{x,\mu\nu}$ penetrating plaquette $(x,x+\mu,x+\mu+\nu,x+\nu)$,

$$\Theta_{x,\mu\nu} \equiv \theta_{x\mu} + \theta_{x+\mu,\nu} - \theta_{x+\nu,\mu} - \theta_{x\nu}, \quad (-4\pi < \Theta_{x,\mu\nu} < 4\pi). \quad (6.1)$$

We decompose $\Theta_{x,\mu\nu}$ into its *integer* part $2\pi n_{x,\mu\nu}$ ($n_{x,\mu\nu}$ is an integer) and the remaining part $\widetilde{\Theta}_{x,\mu\nu} \equiv \Theta_{x,\mu\nu}(\mathrm{mod}\,2\pi)$ uniquely,

$$\Theta_{x,\mu\nu} = 2\pi n_{x,\mu\nu} + \widetilde{\Theta}_{x,\mu\nu}, \quad (-\pi < \widetilde{\Theta}_{x,\mu\nu} < \pi). \quad (6.2)$$

Physically, $n_{x,\mu\nu}$ describes the Dirac string whereas $\widetilde{\Theta}_{x,\mu\nu}$ describes the fluctuations around it. The quantized instanton charge Q_x at the cube around the site $\tilde{x}=x+\frac{\hat{1}}{2}+\frac{\hat{2}}{2}+\frac{\hat{3}}{2}$ of the dual lattice is defined as

$$Q_x = -\frac{1}{2}\sum_{\mu,\nu,\rho} \epsilon_{\mu\nu\rho}(n_{x+\mu,\nu\rho}-n_{x,\nu\rho})$$

$$= \frac{1}{4\pi}\sum_{\mu,\nu,\rho} \epsilon_{\mu\nu\rho}(\widetilde{\Theta}_{x+\mu,\nu\rho}-\widetilde{\Theta}_{x,\nu\rho}), \quad (6.3)$$

where $\epsilon_{\mu\nu\rho}$ is the complete antisymmetric tensor. Q_x measures the total flux emanating from the monopole (instanton) sitting at $\tilde{x}$. Roughly speaking, Q_x measures the strength of nonperturbative gauge configurations. Polyakov showed that a condensation of these instantons drives the system at $c_1=0$ into a confinement phase, which is characterized by strong and large fluctuations of gauge field $\theta_{x\mu}$ at long distances.

B. Results

In this subsection, we shall show "snapshots" of Q_x, typical configurations of Q_x taken in the process of MC updates after sufficient thermalization. In Fig. 14, we first show the locations of pairs of (c_2,c_1) in the phase diagram at which snapshots are taken. In Fig. 15, we present the snapshots at these locations for the lattice $N=16^3$. In Fig. 16, we show $Q(n)$, the density of instantons with the charge $n(\geq 0)$,
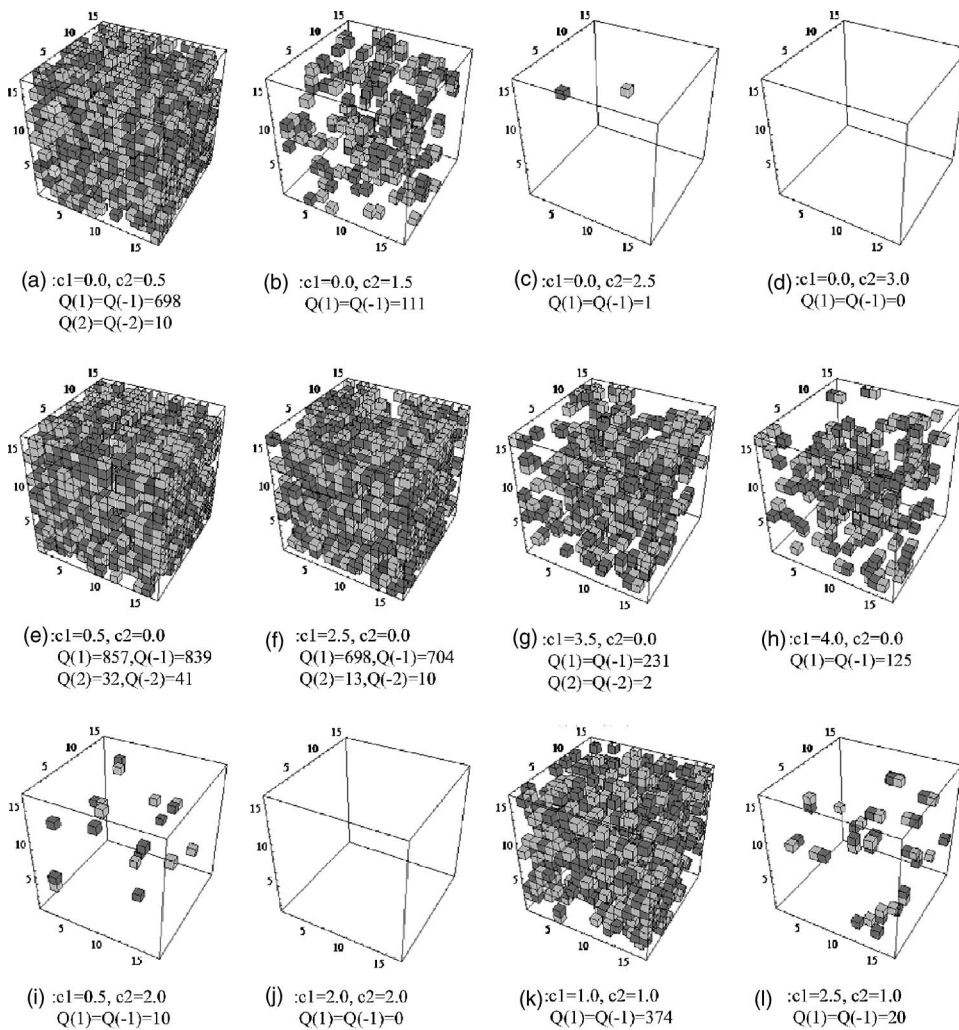
(a) :c1=0.0, c2=0.5
Q(1)=Q(-1)=698
Q(2)=Q(-2)=10

(b) :c1=0.0, c2=1.5
Q(1)=Q(-1)=111

(c) :c1=0.0, c2=2.5
Q(1)=Q(-1)=1

(d) :c1=0.0, c2=3.0
Q(1)=Q(-1)=0

(e):c1=0.5, c2=0.0
Q(1)=857,Q(-1)=839
Q(2)=32,Q(-2)=41

(f) :c1=2.5, c2=0.0
Q(1)=698,Q(-1)=704
Q(2)=13,Q(-2)=10

(g) :c1=3.5, c2=0.0
Q(1)=Q(-1)=231
Q(2)=Q(-2)=2

(h):c1=4.0, c2=0.0
Q(1)=Q(-1)=125

(i) :c1=0.5, c2=2.0
Q(1)=Q(-1)=10

(j) :c1=2.0, c2=2.0
Q(1)=Q(-1)=0

(k):c1=1.0, c2=1.0
Q(1)=Q(-1)=374

(l) :c1=2.5, c2=1.0
Q(1)=Q(-1)=20

FIG. 15. Snapshots of spatial distribution Q_x of instantons. Dark boxes indicate the locations of $Q_x>0$ whereas light boxes indicate $Q_x<0$. $Q(n)=\Sigma_x\delta_{n,|Q_x|}$ is the density of instantons with the charge n.

$Q(n)=\Sigma_x\delta_{n,|Q_x|}/N$. The length of each hexahedron shows the magnitude of instanton charges there.

Let us first see the behavior of instantons in the pure 3D U(1) gauge system with $c_1=0$ [Figs. 14(a)–14(d)]. The result indicates that the instanton density decreases very rapidly from $c_2\sim1.5$ as c_2 increases. Therefore we can identify the crossover found by the specific heat C in Sec. IV as a crossover from the region of dense instantons to that of dilute instantons. In fact this was earlier observed in Ref. 17.

More systematically, we calculate the average density, $\rho\equiv\langle\Sigma_x|Q_x|\rangle/N$ for $c_1=0$ as a function c_2; see Fig. 17. We fit the result with $\exp(-\ell c_2)$ as expected by the dilute-gas approximation,[10] where $\ell\simeq4.35$, whereas its theoretical value is calculated as 5.06.[10] The fitting is quite satisfactory for $c_2>1.5$ as expected.

Let us turn to the pure CP^1 model at $c_2=0$. In Fig. 15, the snapshots (e)–(h) represent this case. The c_1 term of the action shows that a spin order, i.e., a condensation of z_x, suppresses the fluctuations of $U_{x\mu}$. Due to this correlation $\bar{z}_{x+\mu}z_x\leftrightarrow U_{x\mu}$, instanton configurations in (2+1) dimensions correspond to creations and/or destructions of so-called skyrmion configurations of O(3) spins in the 2D plane. Therefore instantons are suppressed in the spin-ordered state. The results in Fig. 15 are consistent with the above observation as
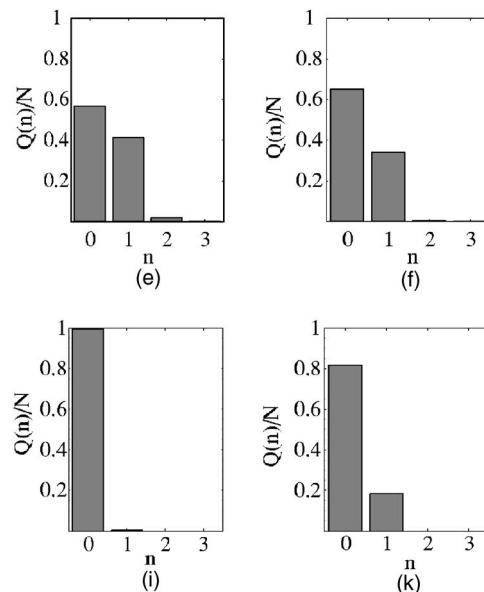

FIG. 16. Distribution of the instanton charge density $Q(n)$ at the locations (e)–(k) in the phase diagram. $Q(n\geq3)=0$.
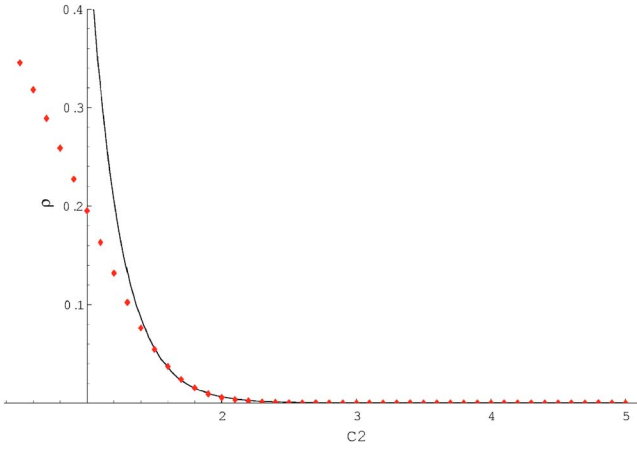
FIG. 17. (Color online) Average of instanton density ρ $=\langle\Sigma_x|Q_x|\rangle/N$ for $c_1=0$ as a function of c_2. The solid curve is a fit in the form of dilute-gas approximation $\propto\exp(-\ell c_2)$ with $\ell\simeq4.35$.

the instanton density decreases as c_1 increases. However, we note that even in the spin-ordered phase at $c_1=3.5$ there are a number of surviving instantons, most of which make instanton–anti-instanton dipoles in the nearest-neighbor pairs.

Finally, let us take a look at the snapshots obtained in the region close to the critical line; the snapshots at (i)–(l) in Fig. 15. We see that the instanton density increases as c_1 and/or c_2 decrease. Even in the spin-ordered phase, the instanton density is finite for small c_2. We do *not* think that this result contradicts a natural belief that the Higgs phase is realized in the spin-ordered phase. For the confinement phase to appear, finite instanton density is not sufficient, but dissociations of instanton–anti-instanton dipoles are necessary.

The observation of instantons in the present section is quite helpful for understanding the behavior of gauge-boson mass, which is calculated in the following section.

VII. MASS OF GAUGE BOSONS

In this section we study the gauge-invariant mass M_G of gauge bosons. The present model contains two independent dynamical variables, i.e., the CP^1 field and the gauge field, and therefore there exist two independent length scales. In Sec. V, we studied the correlation length of the CP^1 spin sector. In this section, we investigate that of the gauge sector.

We explain the definition of M_G in Sec. VII A, and show the numerical result of M_G in Sec. VII B. In Sec. VII C we address the problem of whether the system is in the confinement phase or in Coulomb phase just on the critical points c_{1c}. In Sec. VII D, we study the case of noncompact gauge field to support our argument for the problem in Sec. VII C.

A. Definition of gauge-boson mass M_G

In this section, we study the gauge-invariant mass of gauge bosons, M_G, by using the same techniques that we used to measure the spin gap M_S in the previous section. To define M_G we first introduce a gauge-invariant operator $O(x)$,
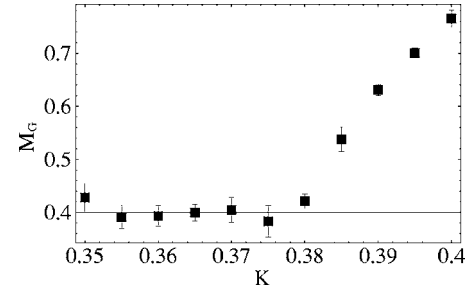

FIG. 18. Gauge-boson mass of Eq. (7.5) for $\beta=2$ and $\lambda=0.020$, the same parameters as in Ref. 18.

$$O(x) = \sum_{\mu,\nu=1,2} \epsilon_{\mu\nu}\mathrm{Im}\,\bar{U}_{x\nu}\bar{U}_{x+\nu,\mu}U_{x+\mu,\nu}U_{x\mu}$$

$$= \sum_{\mu,\nu} \epsilon_{\mu\nu}\sin(-\theta_{x\nu} - \theta_{x+\nu,\mu} + \theta_{x+\mu,\nu} + \theta_{x\mu}). \quad (7.1)$$

Then we introduce a Fourier transform as before,

$$\tilde{O}(x_3) = \sum_{x_1,x_2} O(x)e^{ip_1x_1+ip_2x_2}, \quad (7.2)$$

to define the gauge correlation function as

$$D_G(t) = \frac{1}{L^3}\sum_{x_3} \langle\tilde{O}(x_3)\bar{\tilde{O}}(x_3+t)\rangle. \quad (7.3)$$

In the continuum, $D_G(t)$ is expected to behave as

$$D_G(t) = \int dp_3 \frac{e^{ip_3t}}{\vec{p}^2 + M_G^2} \propto e^{-\sqrt{p_1^2+p_2^2+M_G^2}t}. \quad (7.4)$$

We determine M_G by fitting the data in this exponential form (7.4). For practical calculations, we set $p_1=p_2=2\pi/L$ as before. Here we note that we are assuming the ordinary form of the gauge-boson propagator for a gauge system coupled with *massive* matter fields. *On the critical line*, the gauge-boson propagator may be modified due to the appearance of massless field z_{xa}. See later discussion on this point.

In order to verify that the above methods give correct results, we first apply them to the 3D U(1) lattice gauge-Higgs models for which the gauge-boson mass has been already calculated by using other methods. In Ref. 18 the action S of the model is parametrized as follows;

$$S_{Ch} = -\frac{\beta}{2}\sum_P \prod U - \frac{K}{2}\sum_{x,\mu} (\bar{\Phi}_{x+\mu}U_{x\mu}\Phi_x + \mathrm{H.c.})$$

$$+ \sum_x [|\Phi_x|^2 + \lambda(|\Phi_x|^2 - 1)^2], \quad (7.5)$$

where Φ_x is the complex Higgs field. By changing the value of K, the system undergoes a Higgs-confinement phase transition. A gauge-boson mass was calculated by studying the *genuine gauge-boson propagator* with a specific gauge-fixing condition. We calculated the gauge boson mass for the same parameter region as in Ref. 18 but by using $D_G(t)$ of Eq. (7.3). In this region, the gauge coupling constant has a moderate value $\beta=2$ and $\lambda=0.020$. In Fig. 18 we show our results of the gauge-boson mass, which are in good agree-
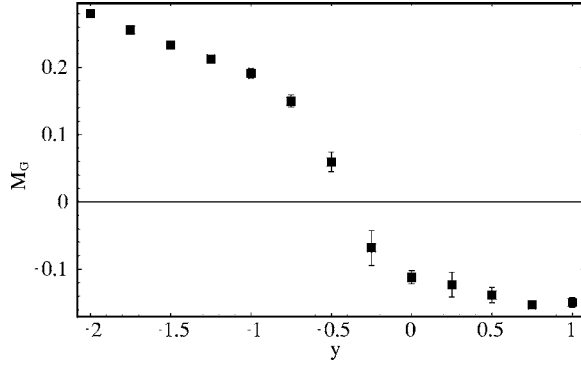
FIG. 19. Gauge-boson mass of Eq. (7.6) for $x=2$, $\beta=4$, and $K=5$, the same parameters as in Ref. 19. Here and in the forthcoming figures of M_G, M_G denotes the product sgn$(M_G^2)\sqrt{|M_G^2|}$ with M_G^2 defined by Eq. (7.4) in order to distinguish the case of negative M_G^2 clearly.

FIG. 20. Gauge-boson mass M_G as a function of c_2 for $c_1=0.0$, 0.8, 1.5. The data of $c_1=0.0$ and 0.8 almost overlap.

ment with those of Ref. 18. We should notice that the gauge boson mass is always nonvanishing even at the critical point, though one might expect the behavior $M_G^2 \sim |K-K_c|$ where K_c is the value at the critical point. We shall comment on this point after showing the results of the present CP^1+U(1) model.

On the other hand, in Ref. 19, it was reported that the gauge-boson mass vanishes in a certain parameter region. In Ref. 19, the Higgs part of the action is parametrized in a complicated way as

$$S_{Ka} = -\frac{\beta}{2}\sum_P \prod U - \frac{K}{2}\sum_{x,\mu}(\bar{\Phi}_{x+\mu}U_{x\mu}\Phi_x + \text{H.c.})$$
$$+ \frac{K}{2}\sum_x |\Phi_x|^2 \left(6 + \frac{y}{K^2} - \frac{3.17(1+2x)}{2\pi K}\right.$$
$$\left. - \frac{(-4+8x-8x^2)(\log 6\beta + 0.09) + 25.5 + 4.6x}{16\pi^2\beta^2}\right)$$
$$+ \frac{xK^2}{4\beta}\sum_x |\Phi_x|^4. \tag{7.6}$$

We also calculated the gauge-boson mass of Eq. (7.6). In Fig. 19 we present our result of M_G for $x=2$, $\beta=4$, and $K=5$, the same parameters used in Ref. 19. The result agrees with that of Ref. 19. For positive y, M_G reduces to around zero. This phenomenon may be understood naturally as follows: for large y the mass term of Φ_x becomes large and Φ_x fluctuates weakly around zero. Then one can treat the hopping K term as a small perturbation. The main term is the first β term whose coefficient is large. Thus the fluctuations of gauge bosons are strongly suppressed, so one can expand as $U_{x\mu} \simeq 1 + iA_{x\mu}$. The resulting action $\propto \Theta_{x,\mu\nu}^2$ describes just free massless gauge bosons. See also the discussion in the following subsection.

B. Case of compact U(1) gauge field

We measured the gauge-boson mass for the 16^3 lattice. So the distance t in $D_G(t)$ of Eq. (7.4) takes $t=1,\ldots,8$ due to the
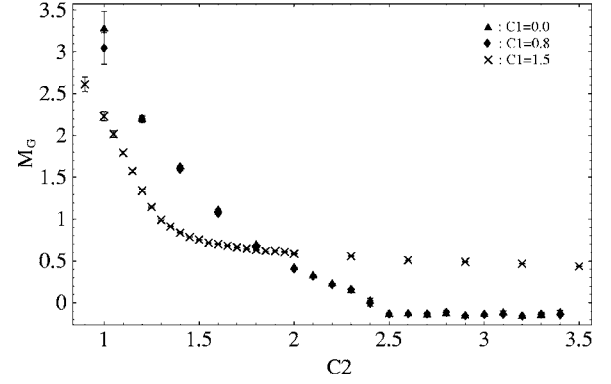
PBC. The value of M_G for each point of the c_2-c_1 plane is calculated as the average of ten samples, each sample of which is obtained after $2\times10^5 \sim 4\times10^5$ sweeps. The error of M_G is evaluated by the standard deviation of these ten samples.

There are two mechanisms to generate nonvanishing M_G: (i) condensation of instantons and (ii) Anderson-Higgs mechanism. We shall see them first by studying $M_G(c_2)$ as a function of c_2 for a fixed c_1, and then by studying $M_G(c_1)$ for a fixed c_2.

In Fig. 20 we present $M_G(c_2)$ for $c_1=0$, 0.8, and 1.5. Let us first see the pure gauge case $c_1=0$ in some detail. As c_2 increases from zero, M_G decreases and becomes almost zero at $c_2\simeq2.5$, the value at which the instanton density almost vanishes. Thus we find a positive correlation between the gauge-boson mass and the instanton density. Actually, in the dilute-gas approximation, M_G is estimated as $M_G\propto\rho \propto\exp(-\ell c_2)$.[10] In fact, for $\rho\simeq0$, one may forget the nonperturbative (instanton) effect and expands as $U_{x\mu}\simeq1+i\theta_{x\mu}$ in the action. The action of small fluctuations $\theta_{x\mu}$ becomes $S \simeq\Sigma_{x\mu\nu}\Theta_{x\mu\nu}^2$, which describe a free massless gauge boson as explained before in the case of Higgs model.[19] On the other hand, for the system of dense instantons, the gauge field $\theta_{x\mu}$ has short-range, i.e., massive, correlations because of their wild fluctuations. In short, as the c_2 term controls the density of instantons, i.e., wild fluctuations of $\theta_{x\mu}$, $M_G(c_2)$ decreases as c_2 increases. Figure 20 shows that this tendency survives for $c_1=0.8$ and 1.5. This is expected from Fig. 15 of instanton density. We remark here that the vanishing gauge-boson mass in the numerical calculations in *finite systems* does *not* guarantee that the system is in the *deconfinement* phase. The measurement of the specific heat indicates that the system is in the confinement phase even for large c_2 if c_1 is below $c_{1c}(c_2)$. We think that the above calculation $M_G\sim0$ in the confinement phase is a finite-size effect and if we calculate M_G in very large systems, we obtain $M_G>0$ in the confinement phase.

In order to verify the above expectation, let us take a look at Fig. 20 in more detail. One sees that $M_G^2=-(0.1)^2 - (0.15)^2$ for $c_2>2.5$ with $c_1=0$ and $c_1=0.8$. As mentioned below Eq. (5.7), these negative values of M_G^2 are possible in the present definition of M_G^2. We think that this unphysical result stems from the finite size of the system as mentioned
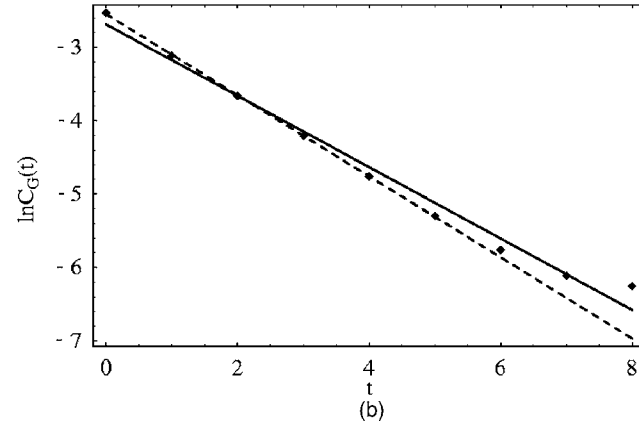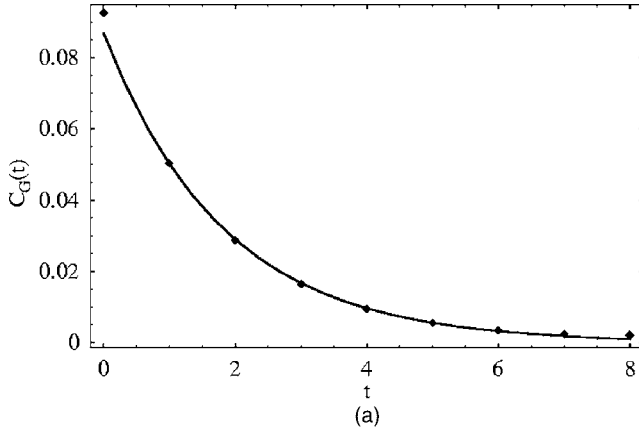
FIG. 21. Correlation function $D_G(t)$ of gauge boson vs t at (c_1 =0.0, c_2=3.0) for L=16. (a) the exponential curve fitting the data with t=0 dropped. (b) Log plot $\ln D_G(t)$. The solid straight line fits all the data, while the dashed straight line fits the data with t=6, 7, 8 dropped.

above. Similar results are reported in Ref. 20 for the D=4 compact scalar QED. In order to see the finite-size effect on the gauge boson mass, we plot data of $D_G(t)$ in the t $-\ln D_G(t)$ plane in Fig. 21. From this plot, it is obvious that the PBC affects the behavior of $D_G(t)$ for $t\sim L/2$ where L is the system size. Then one may discard the data of $t\sim L/2$ and re-estimate the gauge-boson mass to obtain $M_G^2=$ $-(0.08)^2$. To get a definite conclusion for the negative gauge boson mass, calculation in larger systems is required. In this
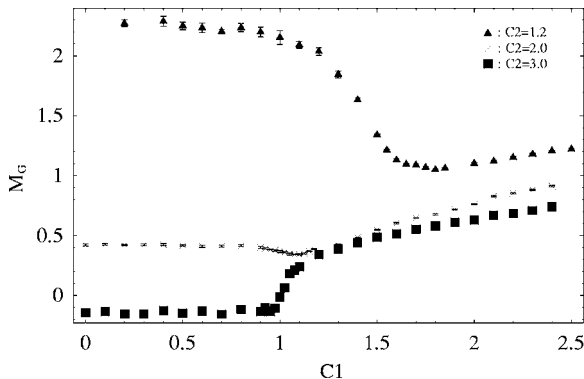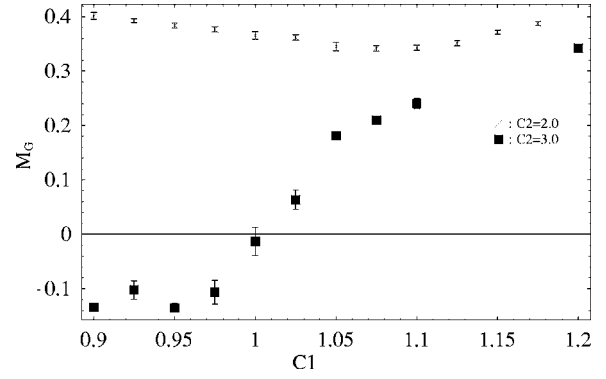

FIG. 22. Gauge boson mass vs c_1 for fixed c_2's.

FIG. 23. Magnified figure of Fig. 22 near the critical line.

direction, we calculated M_G in a larger system 24^3 and obtained a reduced value $M_G^2\sim-(0.03)^2$. Therefore we expect that we obtain $M_G^2\gtrsim0$ by calculation in very large systems, and in particular $M_G^2>0$ in the confinement phase as it is generally expected.

On the other hand, the data for c_1=1.5 are interesting because the horizontal line with c_1=1.5 in the c_2-c_1 plane intersects the critical line as c_2 is increased. The intersection point is estimated as (c_1=1.5, c_2=1.2) from the phase diagram Fig. 8. As seen in Fig. 20, the gauge boson mass decreases very rapidly until $c_2\sim1.3$ and becomes almost constant for $c_2>1.4$. This rapid decrease of M_G in the spin-disordered phase comes from the decrease of the instanton density as we measured in the previous section. The finite gauge-boson mass in the spin-ordered phase can be interpreted as due to the *Anderson-Higgs mechanism* because M_G stays almost constant for varying c_2. We shall explain this mechanism in more detail for $M_G(c_1)$ below.

Next, let us study $M_G(c_1)$ for a fixed c_2. In Figs. 22–26, we present $M_G(c_1)$. For all values of c_2, as c_1 increases from zero, $M_G(c_1)$ first decreases in the spin-disordered (confinement) phase, $0<c_1<c_{1c}(c_2)$, to reach the minimum at the critical point $c_1=c_{1c}(c_2)$. Then it increases in the spin-ordered (Higgs) phase $c_{1c}(c_2)<c_1$. The first decrease is due to the suppression of instantons at larger c_1 as we observed in the previous section. The situation parallels the pure gauge system c_1=0 if the axes c_1 and c_2 are interchanged.

The successive increase in the ordered phase is due to the Anderson-Higgs mechanism. In the ordered phase, $\langle z_x\rangle$ starts
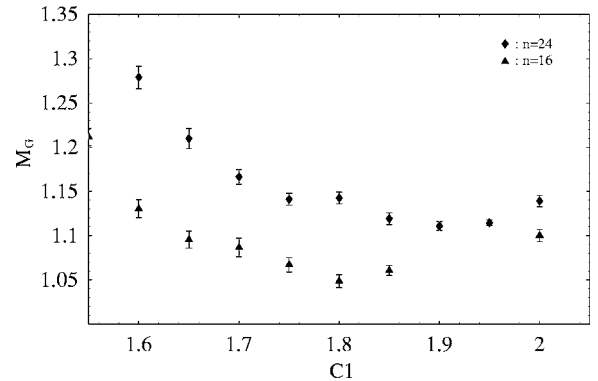

FIG. 24. Size dependence of the gauge-boson mass with c_2 =1.2.
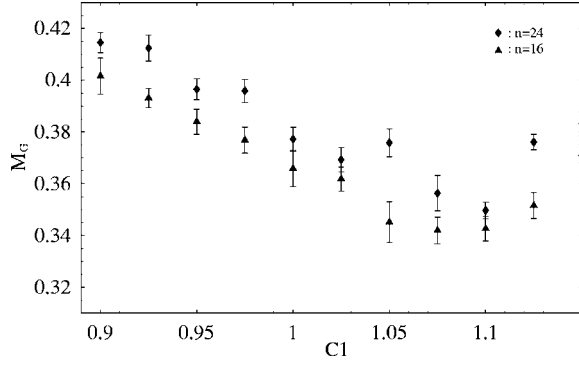
FIG. 25. Size dependence of the gauge-boson mass with c_2 =2.0.

to develop at $c_1=c_{1c}$ as Fig. 10 shows. Then the c_1 term of the action supplies the following mass term:

$$S_M = \frac{1}{2} M_G^2 \sum_{x\mu} \theta_{x\mu}^2, \quad M_G^2 = c_1 \langle z_x \rangle^2, \quad (7.7)$$

where we expanded $U_{x\mu} \simeq 1 + i\theta_{x\mu}$ by assuming small gauge-field fluctuations $\theta_{x\mu}$. This expression M_G at a fixed c_2 certainly increases as $c_1(>c_{1c})$ increases.

An important point is that the gauge boson mass is *non-vanishing* on the critical line except for relatively large values of c_2. To confirm this point we present the size dependence of M_G in Figs. 24–26. They show that M_G slightly increases for a larger lattice, which denies the possibility that $\text{Min}[M_G(c_1)] \to 0$ as $L \to \infty$. This point is in contradiction to the expression (7.7), where $\langle z_x \rangle^2 = 0$ at $c_1 = c_{1c}$ implies $M_G(c_{1c}) = 0$. The nonperturbative effects of $U_{x\mu}$ are crucial to explain $M_G \neq 0$. In fact, we observe M_G at the criticality increases as c_2 decreases. This behavior is consistent with the result of the instanton density at $c_1 = c_{1c}$, which is nonvanishing and increases as c_2 decreases. This suggests that on the critical line, the *confinement phase* in which instantons survive, rather than the Higgs or Coulomb phases, is realized. In a later subsection, we shall confirm this point by studying the noncompact version of the present model. Here we note that the fact $M_G(c_{1c}) \neq 0$ does not contradict the general property of a second-order transition that the correlation length diverges at a critical point. In fact, we have observed in Fig. 13
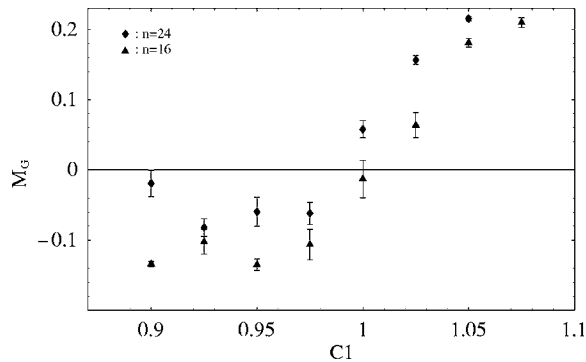

FIG. 26. Size dependence of the gauge-boson mass with c_2 =3.0.

that the spin gap M_S vanishes at $c=c_{1c}$. Thus the spin-correlation length diverges on the critical line, which is sufficient to generate singularities in thermodynamic quantities, although the gauge correlation length is finite there.

C. Confinement phase vs Coulomb phase on the critical line

Physical properties of a quantum system just on its critical point are interesting. For example in the previous paper,[11] by a gauge-theoretical study of a quantum spin system having a Néel-dimer (Higgs-confinement) transition, we argued that the Coulomb-like phase is realized on the critical point. This is because there appears massless relativistic spinon z_{xa} on the critical point and it generates nonlocal correlations for the gauge field. The typical form of the effective gauge model is given as

$$S_{\text{eff}} = g_e \sum_{\mathcal{C}} \gamma^{|\mathcal{C}|} \prod_{\mathcal{C}} U, \quad (7.8)$$

where $\mathcal{C}$ denotes an arbitrary closed loop on the lattice and $|\mathcal{C}|$ is its length. g_e is the effective gauge coupling constant and γ is a parameter of the hopping expansion. At the critical value $\gamma = \gamma_c$, which corresponds to relativistic massless matter fields, S_{eff} diverges for the uniform configuration $U_{x,\mu}$ =1. Recently we studied models closely related to Eq. (7.8) and showed that there exists a deconfinement phase transition at $\gamma = \gamma_c$ and sufficiently large g_e.[21] *In the deconfinement phase*, the renormalized gauge boson propagator behaves at long distance $p \sim 0$ as follows:

$$\langle A_\mu(-p)A_\nu(p)\rangle \sim \frac{1}{\sqrt{p^2}} \delta_{\mu\nu}, \quad (7.9)$$

which gives potential energy between charges at distance r as $1/r$. Then we should evaluate the following Fourier integral instead of Eq. (7.4):

$$F(p_1^2 + p_2^2; t) = \int dp_3 \frac{e^{ip_3 t}}{\sqrt{\vec{p}^2 + M^2}}. \quad (7.10)$$

We numerically evaluated the above integral (7.10) and found

$$F(\ell; t) \sim e^{-\alpha_0 \sqrt{\ell + M^2} t}, \quad \alpha_0 \sim 1.287 \ldots. \quad (7.11)$$

One may expect that the above change of the fitting function $F(\ell; t)$ may explain the finiteness of the gauge-boson mass at the criticality. However, this is not the case. Let us assume $M_G = 0$ on the critical line in the present model. Then the correlation function of $\tilde{O}(x_3)$ obtained by the propagator (7.9), $D_G'(t)$, behaves as

$$D_G'(t)\big|_{M_G=0} \sim e^{-\alpha_0 \sqrt{p_1^2 + p_2^2} t}. \quad (7.12)$$

From Eq. (7.12) it is obvious that the function $D_G'(t)\big|_{M_G=0}$ is *invariant* under a *scale transformation*; $(t, \vec{p}) \to (\xi t, \vec{p}/\xi)$ where ξ is a parameter of the scale transformation. This means that if $M_G = 0$ and the "Coulomb phase" is realized at the critical line, the damping factor of $D_G(t)$ stays *constant* along the critical line. However, in Fig. 22, the value of M_G
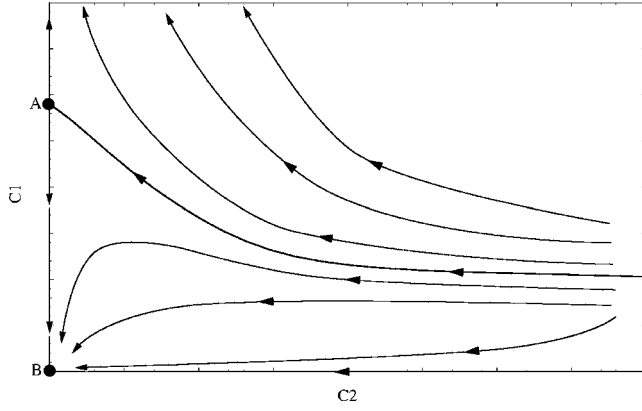
FIG. 27. Renormalization-group flow in the phase diagram. The thick line is the critical line. A is an unstable fixed point, and B is a stable fixed point where density of instantons diverges.

at minimum (which gives the damping factor) clearly increases as c_2 decreases. This implies that there exists a physical scale of the mass dimension (i.e., the gauge-boson mass M_G) in the gauge-boson sector at the criticality, which supports the conclusion in the previous section that $M_G \neq 0$ on the critical line.

In Fig. 27 we present the suggested flow diagram of the renormalization group (RG) in the present model. The RG flow on the *critical line* moves toward the unstable fixed point A in the phase diagram. The two flow diagrams Figs. 2 and 27 are quite similar; the unstable fixed point ($s=s_c, f=0$) in Fig. 2 corresponds to point A in Fig. 27, and similarly the Néel point to the point ($c_2=0, c_1=\infty$), the VBS to point B ($c_2=c_1=0$), and the U(1) spin liquid to the point ($c_2=\infty, c_1=0$). More comments on this point will be given in Sec. VIII.

D. Case of noncompact U(1) gauge field

For the U(1) gauge-Higgs model on a 3D lattice, exactly the same behavior of the gauge-boson mass as ours was observed in the parameter region near the continuous phase transition.[18,22] In Ref. 22, by using the gauge fixing condition, the gauge field propagator is investigated. There the gauge field was split into a singular (instanton) part and the remaining regular part. On the critical line and also in the confinement phase it was shown that the propagator of the regular part has a vanishing mass, whereas the full propagator has a finite mass. From this observation, it is obvious that the finite mass at the criticality stems from the instanton gas.

In order to check whether the above observation[18,22] on the generation of gauge-boson mass on the critical line can be applicable also to the present model, one needs to separate the effect of nonperturbative instanton effects. In Ref. 24 the related work was reported for the O(3) sigma model, in which the effect of nonperturbative spin configuration was studied by suppressing the hedgehog configurations. Below we study this problem by considering the *noncompact* U(1) gauge theory of the CP^1 Schwinger bosons directly and compare the results with those of the compact U(1) system. The action of the noncompact model is given by
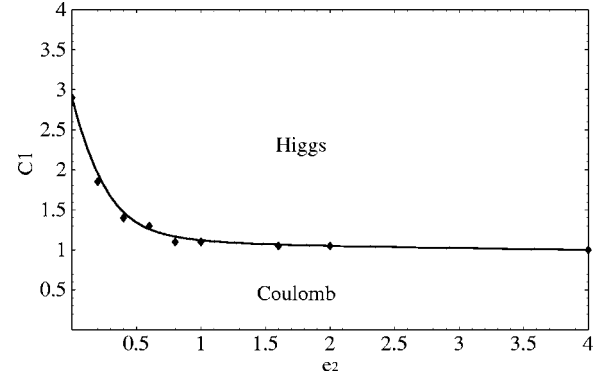

FIG. 28. Phase diagram of the noncompact gauge model. In the noncompact case, the region of the ordered-Higgs phase is enlarged by the suppression of gauge-field fluctuations. The crossover line from the dense to dilute instanton regions disappears.

$$S = -\frac{c_1}{2} \sum_{x,\mu,a} (\bar{z}^a_{x+\mu,a} U_{x,\mu} z_{xa} + \text{H.c.} .) + \frac{e_2}{2} \sum_x \sum_{\mu<\nu} (\Theta_{x,\mu\nu})^2,$$

(7.13)

where $\Theta_{x,\mu\nu}$ is defined by Eq. (6.1) and the constant e_2 controls fluctuations of the noncompact gauge field. For small fluctuations of gauge field, $|\Theta_{x,\mu\nu}| \ll 1$, hence the two models are almost equivalent under the relation $e_2 \sim c_2$.

In Fig. 28 we present the phase diagram of the model (7.13) obtained by calculating the specific heat. The crossover line in the compact case disappears as we expect from the discussion on the instanton. The region of the ordered-Higgs phase is enlarged by the suppression of fluctuations of $\theta_{x\mu}$.

In Fig. 29 and 30 we present the gauge-boson mass M'_G calculated as in the compact case. It is obvious that $M'_G \sim 0$ in the disordered phase, and it starts to increase at the critical point as expected. Its behavior in the ordered-Higgs phase is more or less similar to that of the compact gauge model.

Then we are interested in the instanton density in the noncompact model. From the definition of the instanton density (6.3), it is obvious that instantons *can be generated* even in the noncompact model. In Fig. 31 we compare the instanton
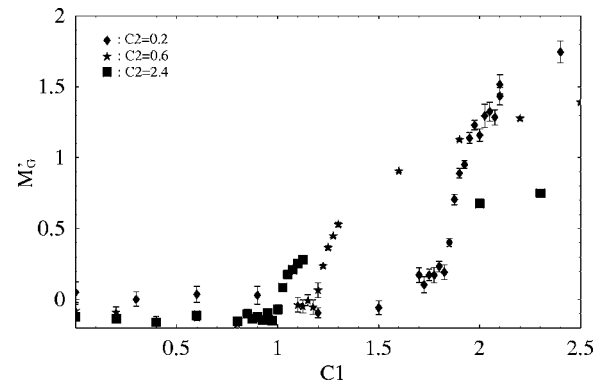

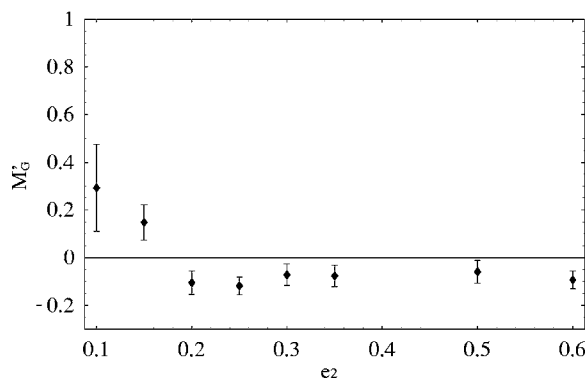FIG. 29. Gauge-boson mass in the noncompact gauge model as a function of c_1.

FIG. 30. Gauge-boson mass in the noncompact gauge model as a function of c_2 with $c_1=0$.

FIG. 32. Gauge-boson mass near the critical points in CP^N(N =1–4) models.

density in the two models: $\rho(c_2)$ in the compact model and $\rho'(e_2)$ in the noncompact model.

From the results, it is easily seen that $\rho'(e_2)$ in the noncompact gauge model is smaller than $\rho(c_2)$ in the compact model as expected. However, there exists a number of instantons for small e_2 (i.e., large gauge coupling) and one may wonder whether a confinement phase exists for sufficiently small e_2. The observation of the specific heat and the gauge-boson mass of course denies this possibility.

From the studies on the noncompact gauge theory in this subsection, it is obvious that the observed nonvanishing gauge-boson mass on the critical line of the compact gauge theory stems from the existence of instantons and not the Anderson-Higgs mechanism.

VIII. DISCUSSION

In this paper, we have introduced 3D CP^1+U(1) lattice gauge theory and studied its phase structure intensively. The specific heat exhibits a second-order phase transition at c_1 =$c_{1c}(c_2)$. The O(3) spin correlation functions show that this critical point separates the spin ordered and disordered phases. The universality class changes from the O(3) spin model at $c_2=0$ to the O(4) spin model $c_2=\infty$ smoothly. The MFT interprets the spin ordered phase as the Higgs phase and the spin disordered phase as the confinement phase. The
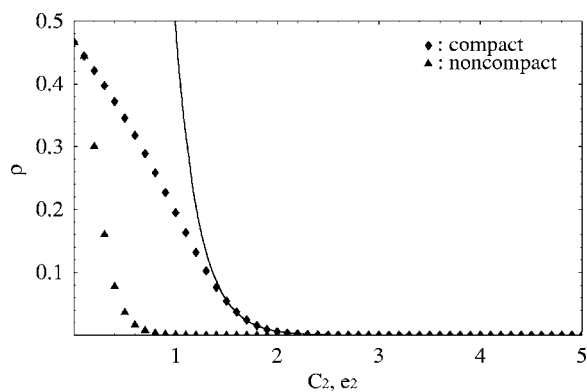

FIG. 31. Instanton density in compact and noncompact U(1) gauge theories. The solid curve is a fit $\rho \propto \exp(-\ell c_2)$
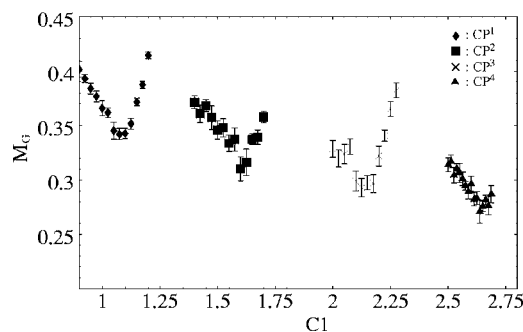
distributions of instantons are studied, which provides us with a rough image of gauge-field configurations in various points in the c_2-c_1 plane. The gauge-invariant mass M_G of gauge boson has two origins: (i) condensation of instantons in the confinement phase and (ii) Anderson-Higgs mechanism (condensation of the CP^1 field) in the Higgs phase. As explained above, the conventional MFT plus one-loop correction like Eq. (7.7) predicts that $M_G=0$ on the critical points. However, we observed $M_G \neq 0$ at $c_1=c_{1c}$ due to the remaining instantons. This suggests that the system is in the confinement phase just on $c_1=c_{1c}(c_2)$. $M_G(c_{1c}) \neq 0$ is compatible with the second-order phase transition because the spin gap $M_S(c_{1c})=0$.

In our recent paper,[21] we introduced a 3D nonlocal U(1) lattice gauge theory, which is obtained by mimicking the effect of massless (gapless) matter fields in a form similar to the gauge model Eq. (7.8). This model contains an inverse gauge coupling g_e, which is proportional to the number of massless matter fields. By studying it numerically, we found that there exists a deconfinement phase transition at a critical gauge coupling $g_e=g_{ec}$. This result suggests that a similar deconfinement phase may appear on the critical points in the present model if the number of matter fields increases as CP$^1 \rightarrow$ CP^N (N=large). This possibility is also consistent with the recent analytical studies on the massless QED$_3$ which suggests that a deconfinement phase is realized for a sufficiently large number of massless fermions.[23]

From these motivations, we numerically studied the CP^N +U(1) gauge theory with N=2, 3, and 4, in particular its gauge-boson mass. This model has a qualitatively same phase structure as the CP^1+U(1) model but the critical line $c_1=c_{1c}(c_2)$ shifts upward in the phase diagram (shrinkage of the Higgs phase).

In Fig. 32, we compare the gauge-boson mass for N=1, 2, 3, and 4. M_G decreases slightly as N increases but is still nonvanishing. We hope to report on a more systematic study of the CP^N+U(1) model in a future publication.

The present study should certainly shed some light on rich properties of a wide range of quantum spin systems as a good Ginzburg-Landau-type phenomenological model. For example, the observed phase diagram and the study of the instanton in the present CP^1+U(1) model are quite useful to understand the phase structure of the continuum GLT of Eq. (2.17). As pointed out in Sec. VII C, the RG flows in Figs. 2 and 27 are very similar. Furthermore, we note that the instan-

ton distributions in Fig. 16 show that most instantons have topological charges $|Q_x|$ less than 3. For the AF Heisenberg model with ring exchange, it was argued[14] that instantons with $|Q_x|=1$, 2, and 3 do not contribute to disordering the gauge dynamics because of a cancellation mechanism due to the Berry phase. Therefore if there exist the Berry phase term in the action of the present model (2.4), the Coulomb phase is realized on the critical line instead of the confinement phase and the GLT of Eq. (2.17) describes this phase transition.

[1] J. K. Jain, Phys. Rev. Lett. **63**, 199 (1989).

[2] I. Ichinose and T. Matsui, Phys. Rev. B **68**, 085322 (2003); see also the references cited therein.

[3] P. W. Anderson, Phys. Rev. Lett. **64**, 1839 (1990).

[4] I. Ichinose and T. Matsui, Nucl. Phys. B **394**, 281 (1993); Phys. Rev. B **51**, 11860 (1995).

[5] I. Ichinose T. Matsui, and M. Onoda, Phys. Rev. B **64**, 104516 (2001); see also the references cited therein.

[6] See, for example, S. Sachdev, *Quantum Phase Transitions* (Cambridge University Press, Cambridge, England, 1999).

[7] T. Senthil, A. Vishwanath, L. Balents, S. Sachdev, and M. P. A. Fisher, Science **303**, 1490 (2004); X. Liu, D. Mazumdar, B. D. Schrag, W. Shen, and G. Xiao, Phys. Rev. B **70**, 014407 (2004).

[8] T. Senthil, S. Sachdev, and M. Vojta, Physica B **359**, 9 (2004).

[9] I. Ichinose and T. Matsui, Phys. Rev. B **45**, 9976 (1992); H. Yamamoto, G. Tatara, I. Ichinose, and T. Matsui, Phys. Rev. B **44**, 7654 (1991).

[10] A. M. Polyakov, Nucl. Phys. B **120**, 429 (1977).

[11] D. Yoshioka, G. Arakawa, I. Ichinose, and T. Matsui, Phys. Rev. B **70**, 174407 (2004).

[12] D. P. Arovas and A. Auerbach, Phys. Rev. B **38**, 316 (1988).

[13] P. Tomczak and J. Richter, J. Phys. A **34**, L461 (2001), and references cited therein.

[14] N. Read and S. Sachdev, Phys. Rev. Lett. **62**, 1694 (1989); F. D. M. Haldane, Phys. Rev. Lett. **61**, 1029 (1988).

[15] R. P. Feynman, *Statistical Mechanics, A Set of Lectures* (W.A. Benjamin, New York, 1972), Chap. 8.

[16] T. A. DeGrand and D. Toussaint, Phys. Rev. D **22**, 2478 (1980).

[17] R. J. Wensley and J. D. Stack, Phys. Rev. Lett. **63**, 1764 (1989).

[18] M. N. Chernodub, R. Feldmann, E. M. Ilgenfritz, and A. Schiller, Phys. Rev. D **70**, 074501 (2004).

[19] K. Kajantie, M. Karjalainen, M. Laine, and J. Peisa, Phys. Rev. B **57**, 3011 (1998).

[20] H. G. Evertz, K. Jansen, J. Jerák, C. B. Lang, and T. Neuhaus, Nucl. Phys. B **285**, 590 (1987).

[21] G. Arakawa, I. Ichinose, T. Matsui, and K. Sakakibara, Phys. Rev. Lett. **94**, 211601 (2005).

[22] M. N. Chernodub, E.-M. Ilgenfritz, and A. Schiller, Phys. Lett. B **555**, 206 (2003).

[23] H. Kleinert, F. S. Nogueira, and A. Sudbø, Phys. Rev. Lett. **88**, 232001 (2002); Nucl. Phys. B **666**, 361 (2003); F. S. Nogueira and H. Kleinert, cond-mat/0501022; Ki-Seok Kim, cond-mat/0503458.

[24] O. I. Motrunich and A. Vishwanath, cond-mat/0311222, Phys. Rev. B (to be published).